Late Holocene sea-surface temperature and precipitation variability in northern Patagonia, Chile (Jacaf Fjord, 44°S)

Julio Sepúlveda[a,†,*], Silvio Pantoja[b], Konrad A. Hughen[c], Sébastien Bertrand[c,‡], Dante Figueroa[d], Tania León[b], Nicholas J. Drenzek[c], and Carina Lange[b]

[a]Center for Marine Environmental Sciences – MARUM and Department of Geosciences, University of Bremen, Leobener Strasse, MARUM, D-28359 Bremen, Germany

[b]Department of Oceanography and Center for Oceanographic Research in the eastern South Pacific, University of Concepción, P.O. Box 160-C, Concepción, Chile

[c]Department of Marine Chemistry and Geochemistry, Woods Hole Oceanographic Institution, Woods Hole, MA 02543, USA

[d]Department of Geophysics and Center for Oceanographic Research in the eastern South Pacific, University of Concepción, P.O. Box 160-C, Concepción, Chile

[†]Present address: Department of Earth, Atmospheric and Planetary Sciences, Massachusetts Institute of Technology, 45 Carleton Street, E25-623, Cambridge MA 02142, USA

[‡]Present address: Alfred Wegener Institute, Am Handelshafen 12, D-27570 Bremerhaven, Germany

*Corresponding author. E-mail address: juliosep@mit.edu (J. Sepúlveda). Phone: +1 617 324 3954; Fax: + +1 617 253 8630

KEYWORDS: Holocene; Westerly Winds; Chile; Northern Patagonia; Jacaf fjord; precipitation; sea surface temperature; lipid biomarkers

ABSTRACT

A high-resolution multi-proxy study including the elemental and isotopic composition of bulk organic matter, land plant-derived biomarkers, and alkenone-based sea surface temperature (SST) from a marine sedimentary record obtained from the Jacaf Fjord in northern Chilean Patagonia (~ 44°20'S) provided a detailed reconstruction of continental runoff, precipitation, and summer SST spanning the last 1750 years. We observed two different regimes of climate variability in our record: a relatively dry/warm period before 900 cal yr BP (lower runoff and average SST 1°C warmer than present-day) and a wet/cold period after 750 cal yr BP (higher runoff and average SST 1°C colder than present-day). Relatively colder SSTs were found during 750-600 and 450-250 cal yr BP, where the latter period roughly corresponds to the interval defined for the Little Ice Age (LIA). Similar climatic swings have been observed previously in continental and marine archives of the last two millennia from central and southern Chile, suggesting a strong latitudinal sensitivity to changes in the Southern Westerly Winds, the main source of precipitation in southern Chile, and validating the regional nature of the LIA. Our results reveal the importance of the Chilean fjord system for recording climate changes of regional and global significance.

INTRODUCTION

Climate changes occurring during the last two millennia are of particular importance for understanding recent and predicting future abrupt climate changes. The data presently available from this period shows that climate conditions were more variable than previously thought (e.g., deMenocal and Bond, 1997; Mayewski et al., 2004; Moberg et al., 2005). During this interval, the so-called Medieval Warm Epoch, herein referred to as the Medieval Climatic Anomaly (MCA; Stine, 2000), and the Little Ice Age (LIA) are among the best known examples of centennial-scale climate variability (Lamb, 1965). Although these two periods were first identified in Europe and the Northern Hemisphere, growing evidence has shown a more widespread incidence (Thompson et al., 1986; Stine, 1994; Haug et al., 2001), including bipolar connections (Kreutz et al., 1997; Domack and Mayewski, 1999). However, most of the evidence regarding climate variability on this time scale still comes from records from the Northern Hemisphere; data for the middle and high latitudes of the Southern Hemisphere are still scarce. Deciphering climate variability in the Southern Hemisphere and particularly from southern South America — the only continental land mass lying between 38°S and the Antarctic Circle — is crucial for documenting the inter-hemispheric synchronicity of recent abrupt climate changes and thereby determining their ultimate cause(s).

Paleoclimate archives from central-south Chile (33-44°S) obtained from lacustrine sediment cores (Jenny et al., 2002), tree-rings (Villalba, 1994), and marine sediment cores (Lamy et al., 2001; Lamy et al., 2002; Mohtadi et al., 2007; Rebolledo et al., 2008) have been revealed to be highly sensitive to climate variability at both low and high latitudes. The southeast Pacific and southern Chile (south of 40^{o} S) are strongly influenced by the Southern Westerly Winds (SWW). These, in turn, are affected by the strength of the

Subtropical Pacific Anticyclone (SPA) and the position of the Antarctic Convergence, which result in strong latitudinal temperature and precipitation gradients (Strub et al., 1998). Climatic and oceanographic changes during the Late Holocene in central and southern Chile may have been a response to latitudinal shifts of the SWW (e.g., Benn and Clapperton, 2000; Lamy et al., 2001; Jenny et al., 2002; Mohtadi et al., 2007; Rebolledo et al., 2008). Recent studies have demonstrated that fluctuations in El Niño Southern Oscillation (ENSO) activity and associated low latitude climate systems exert a strong control over the climatic variability of northern Patagonia (Lamy et al., 2001; Ariztegui et al., 2007; Mohtadi et al., 2007; Rebolledo et al., 2008). However, paleoclimate records from tree rings (Lara and Villalba, 1993; Villalba, 1994), glacier fluctuations (Luckman and Villalba, 2001), and marine sediment cores (Lamy et al., 2001) illustrate inconsistent results regarding the occurrence of the MCA and the LIA in southern Chile.

The fjords of northern Chilean Patagonia are located at the northern limit of the strongest influence of the SWW. Characterized by high sediment deposition rates of both marine and terrestrial material, this area is highly sensitive to past changes in precipitation-driven continental runoff. Therefore, it is ideally located to reconstruct variations in the strength or latitudinal position of the SWW through time.

Our research aims to unravel climate variability in northern Chilean Patagonia during the last two millennia, and to establish connections with regional and global climate systems. We present the results of a multi-proxy sedimentary record from Jacaf Fjord (Fig. 1) spanning the last 1750 years. We study the elemental and isotopic composition of carbon and nitrogen in bulk organic matter, as well as the mass accumulation rate of long-chain *n*-alkyl lipids, to reconstruct changes in terrestrial input and continental runoff resulting from changes in precipitation. In addition, we use the alkenone UK'_{37} index to derive a record of

92 sea surface temperature (SST). Changes in marine productivity have been addressed in a
93 companion paper using biological proxies (Rebolledo et al., 2008).
94
95 **MATERIALS AND METHODS**
96 *Study area and sampling*
97 The Chilean fjord area extends from the city of Puerto Montt (42°30'S) to Cape
98 Horn (55°58'S), stretching 1,600 km and covering an area of almost 240,000 km^2 (Silva
99 and Prego, 2002). Three main glacial fields and several major rivers incorporate fresh
100 waters into the fjord system, inducing estuarine conditions with a stratified two-layer water
101 column (Silva et al., 1995), and evidencing maximum outflows at 42°, 46° and 50° S
102 (Dávila et al., 2002). Northern Patagonia presents a marine-temperate and rainy climate
103 strongly influenced by the storm track of the SWW (Fig. 1B). Mean annual precipitation is
104 ~3,000 mm $year^{-1}$ and mean annual air-temperature is ~10°C (DGA, 2003). Dense
105 vegetation characteristic of cold, wet climate regimes surrounds the inner fjord area in the
106 form of a temperate evergreen rain forest (e.g., Villagrán, 1988). The vegetation
107 distribution is controlled latitudinally and altitudinally by sharp temperature and
108 precipitation gradients (Abarzúa et al., 2004, and references therein). Marine primary
109 production in the fjord area from 44º to 46º S is less than 50 mg C m^{-2} d^{-1} in winter and up
110 to 390 mg C m^{-2} d^{-1} in spring (Pizarro et al., 2005).
111 The coring site is located in the Jacaf Fjord (Fig. 1b) of northern Chilean Patagonia
112 (44°20.00S, 72°58.15W). This fjord has a SE-NW orientation, a maximum depth of 675 m,
113 and a very rough bottom topography dominated by narrow, shallow sills (Delgado, 2004).
114 Surface sediments in the area contain up to 3.5% organic carbon (Silva et al., 1998), with
115 modern sedimentation rates in the surrounding area of ~0.26 cm yr^{-1} (Salamanca and Jara,

2003; Sepúlveda et al., 2005). Core CF7-PC33 (1.68 m length, 510 m water depth) was retrieved with a gravity corer during the CIMAR-FIORDO 7 expedition (November 2001) onboard the AGOR Vidal Gormaz of the Chilean Navy. Additionally, a box-corer (CF7-BC33; 510 m water depth) was taken and subsampled at 1 cm increments in order to retrieve the surface sediments intact. The gravity core liners were refrigerated at 4 ºC until laboratory analysis. Each core liner was split longitudinally into two halves; one half was used for visual description, magnetic susceptibility, and XRF scanning; the other half was sampled at 1 cm intervals for elemental and isotopic analyses, and at 2-3 cm intervals for lipid biomarker analysis.

The age model of CF7-PC33 is based on linear interpolation between four AMS ^{14}C dates measured on well-preserved terrestrial vegetation fragments (Rebolledo et al., 2008), and covers the period 1750-75 cal yr BP (Table 1; Fig. 2). Linear sedimentation rates calculated for two intervals, before and after 735 cal yr BP, were 0.82 m kyr^{-1} and 1.2 m kyr^{-1}, respectively (Fig. 2). The average sedimentation rate for the entire record was 1 m kyr^{-1}, yielding a decadal resolution of those proxies measured every one centimeter.

Magnetic susceptibility, elemental and stable isotopes analyses

Magnetic susceptibility (MS) was measured every 5 mm on the surface of the split core sections using a Bartington MS2 magnetic susceptibility meter with a MS2E point sensor.

For elemental C/N analysis, sediment samples were freeze-dried, ground, and homogenized in an agate mortar before processing. About 30 mg of sediment were weighed in tin cups and carbonates were removed by acidification with 50% v/v sulfurous acid. Organic carbon (C_{org}), total nitrogen, bulk $\delta^{13}C$, and $\delta^{15}N$ were analyzed at the University

of California Davis Stable Isotope Facility. Analytical standard deviation was 0.04‰ for $\delta^{13}C$ and 0.14‰ for $\delta^{15}N$. The elemental composition has been published elsewhere (Rebolledo et al., 2008).

Lipid biomarkers

Total lipids were extracted from freeze dried sediments in a DIONEX ASE 200 Accelerated Solvent Extraction System using a mixture of CH_2Cl_2:MeOH 9:1 at 100 ºC and 1000 psi. The non-polar and polar fractions were separated in a LC-NH_2 column after eluting with 7 mL CH_2Cl_2:acetone 9:1 and 8 mL 2% formic acid in CH_2Cl_2, respectively. The non-polar fraction was then hydrolyzed by refluxing in 100 mL 0.5 M KOH in methanol plus 20 mL Milli-Q water for 3 h. Saponified extracts were back-extracted with three 10 mL aliquots of hexane in separatory funnels. These extracts were separated into three fractions using small silica gel columns (100-200 mesh, 5% deactivated), where ketones were eluted in the second fraction with CH_2Cl_2:hexane 2:1. The polar fraction was transesterified with 0.5 mL BF3:MeOH at 70°C for 20 min to convert free and esterified fatty acids into fatty acid methyl esters (FAMEs). Twenty mL Milli-Q water and 10 mL hexane were added. The hexane fraction was subsequently removed, concentrated and loaded into a silica gel column (100-200 mesh, 5% water). FAMEs were eluted in the second fraction with 5% ethyl acetate in hexane. This fraction was transferred to a glass vial with inserts and re-dissolved in 50 µL toluene before injection onto the gas chromatograph.

Gas chromatography of alkenones was carried out using a Shimadzu GC17A (version 3) GC coupled with a Shimadzu AOC-201 autosampler with a 30-m Agilent HP-5 column (0.32 mm ID, 0.25 µm film thickness) and a flame ionization detector. Hydrogen

was used as a carrier gas and the column oven temperature was programmed from 50 ºC (1 min) to 120 ºC (30 min) and then 300 ºC (36 min) until the end of the run (71.3 min). Alkenones were identified by their retention times and quantified correcting for the recovery of 5α-cholestane. Gas chromatography of FAMEs was carried out with a 60-m Chrompack capillary column (0.25 mm ID, 0.25 μm film thickness) using an Agilent 6850 GC coupled with an Agilent 6850 autosampler and a flame ionization detector. Hydrogen was used as a carrier gas and the column oven temperature was programmed from 60 ºC (1 min) to 210 ºC (8 min), and to 330 ºC (53 min). C_{16-32} *n*-alkanoic fatty acids were identified by their retention times and quantified by comparison with a mixture of 9 authenticated reference standards.

The average chain length (ACL) index for the most abundant *n*-C_{24-26} alkanoic fatty acids was estimated as ACL = (Σ [C_i] x i)/ Σ [C_i], for i = 24-26, where C_i = concentration of *n*-alkanoic acid containing i carbon atoms. The ACL for the full suite of long-chain FAs (*n*-C_{24} to *n*-C_{34}), as well as other chain length combinations, did not show noticeable variability along the record. We therefore constrained the ACL index to *n*-C_{24-26} alkanoic fatty acids (see discussion below). The carbon preference index (CPI) was estimated as CPI = sum of even C_{24} to C_{34}/sum of odd C_{23} to C_{33} *n*-alkanoic acids.

We calculated the alkenone unsaturation index (UK'_{37}) as UK'_{37} = ($C_{37:2}$)/($C_{37:3}$+$C_{37:2}$), where $C_{37:2}$ and $C_{37:3}$ represent the di- and tri-unsaturated C_{37} alkenones, respectively (Brassell et al., 1986). The UK'_{37} values were converted into temperature by applying the culture calibration of Prahl et al. (1988) (UK'_{37} = 0.034T + 0.039). The analytical error was calculated as 0.045 Uk'_{37} units or 0.17°C, and was based on triplicate measurements of six samples.

The mass accumulation rate of leaf waxes (MAR_{waxes}) was calculated as $MAR_i = C_i$ x DBD x SR; where C_i is the concentration of leaf waxes in a given interval in mg gdw^{-1}, DBD is the dry bulk density in g cm^{-3}, and SR is the linear sedimentation rate in cm y^{-1}.

Statistical analyses

We used XLSTAT Version 2007.4 to perform the correlation analysis and principal component analysis (PCA) of our data. Proxy data (C/N ratio, $\delta^{13}C$, $\delta^{15}N$) were used to study and visualize the correlation between variables indicating changes in the input of terrestrial organic matter. We chose these three parameters because they reflect relative changes in the contribution of allochthonous (terrestrial) organic matter, they are independent of changes in the sedimentation rate, and they are sampled at the same resolution (1 cm). These three parameters have been shown to vary linearly in response to different input of autochthonous (marine) and allochthonous (terrestrial) organic matter in recent sediments of northern Patagonia (Sepúlveda, 2005). Thus, a terrestrial index (TI) obtained from the first component of the PCA was estimated. Two PCAs were performed, one covering the whole record and one encompassing the data before 450 cal yr BP (data not shown); the latter was used to discuss the role of the variability observed in the $\delta^{15}N$ record. The TI was then compared to MAR-dependant proxies.

RESULTS

Magnetic susceptibility, elemental and isotopic composition

The MS susceptibility varies between 31 and 151 x 10^{-6} S.I. (Fig. 3a). A rather steady increase is observed from the base of the record until around 750 cal yr BP; thereafter values remain fairly constant at around 80 x 10^{-6} S.I.

The molar C/N ratio has been recently reported in a companion paper (Rebolledo et al., 2008). Four time slices can be distinguished, separated by abrupt steps in the C/N ratio: (1) 1750-1500 cal yr BP with values close to 10.5; (2) 1400-900 cal yr BP with values between 11.3 and 11.0; (3) a very short period, 890-780 cal yr BP with values ~11.5; and (4) 890-75 cal yr BP, an interval with a slight decreasing trend, with values from 12.2 to 11.5 (Fig. 3b). The C/N ratio has a significant positive correlation with the MAR_{waxes}, and a significant negative correlation with $\delta^{13}C$, $\delta^{15}N$, and the ACL of plant waxes (Table 2).

The $\delta^{13}C$ values, between -23.2 and -22.1‰, are clearly distinguished into two periods marked by different isotopic signals; the interval from 1750 to 778 cal yr BP showed enrichment from -22.5 to -22.1‰, and then an abrupt depletion to values around -22.6‰ occurs in a short time period (Fig. 3c). The interval between 766 cal yr BP and the top of the core starts with rather stable values of ca. -22.7‰ until 580 cal yr BP, and is followed by a decreasing trend toward minimum values in the upper section of the record (-23.1; Fig. 3c). The $\delta^{13}C$ record reveals significant correlations with all other proxies except $\delta^{15}N$ (Table 2). The $\delta^{15}N$ values vary between 7.4 and 9.4‰ (Fig. 3d). Enriched values between 8.1 and 8.5‰ are found before 923 cal yr BP, followed by two abrupt depletions to values about 7.8‰ between 923 and 875 cal yr BP and to about 7.4‰ between 826 and 737 cal yr BP (Fig. 3d). After 737 cal yr BP, values remain low until 550 cal yr BP, when a strong enrichment of ~2‰ starts, reaching maximum values (9.4‰) at ~220 cal yr BP. A quick recovery to more depleted values characterizes the uppermost part of the record (Fig. 3d). The $\delta^{15}N$ record only correlates significantly with the C/N ratio (Table 2). When correlating the variables before 450 cal yr BP, and thus avoiding the marked positive $\delta^{15}N$ excursion (Fig. 3d), $\delta^{15}N$ exhibits significant correlations with all the other variables (Table 2).

235

236 *Principal component analysis and terrestrial index*

237 Factor 1 of the PCA, used as a terrestrial index and based on the C/N ratio, $\delta^{13}C$,
238 and $\delta^{15}N$, explains 53.5% of the variability, with the C/N ratio and the $\delta^{13}C$ yielding the
239 highest factor loadings (Fig. 4). Factor 2 (F2) explains ~32.3% of the variability (85.8% of
240 the cumulative variability) with $\delta^{15}N$ as the main contributor (Fig. 4). Since the $\delta^{15}N$ record
241 has a high impact on factor 2 of the PCA due to the large enrichment observed between 400
242 and 200 cal yr BP, we carried out an additional PCA including only data before 450 cal yr
243 BP. The results of the latter analysis reveal factors 1 and 2 contributing with 70.15 and
244 16.81% of the variability, respectively (86.97% cumulative). The temporal trend of factor 1
245 remains similar for both analyses, corroborating the use of this statistical tool for
246 reconstructing terrestrial input. Negative (positive) values of the graphical expression of the
247 TI are interpreted as a low (high) relative contribution of terrestrial organic matter resulting
248 from decreased (increased) precipitation and continental runoff (Fig. 5a). The TI segregates
249 two intervals separated by a stepwise transition: (a) before 900 cal yr BP, with lowest TI
250 values along the record; and (b) a period after 750 cal yr BP characterized by the highest
251 values of the record (Fig. 5a).

252

253 *Lipid biomarkers and inorganic geochemistry*

254 The concentration of plant waxes varies between 2.35 and 24.18 μg gdw^{-1}, and the
255 MAR fluctuates between 0.93 and 10.80 mg m^{-2} yr^{-1} throughout the core (Fig. 5b). The 3-
256 point running average depicts a rather stable period with lower values (<5 mg m^{-2} yr^{-1})
257 before 1200 cal yr BP followed by an increase from 1200 to 950 cal yr BP. A sharp

decrease occurs at 880 cal yr BP. Values increase again to ~8 mg m^{-2} yr^{-1} until ~700 cal yr BP and remain slightly higher than the older period until the top of the core (Fig. 5b). The ACL_{24-26} varies between 25.5 (before 900 cal yr BP) and 25.2 in the youngest part of the core (Fig. 5c). Sedimentary plant waxes display an even-over-odd predominance with CPI values varying between 2.9 and 3.7, reflecting their dominant land-delivered origin. ACL_{24-26} obtained from the core top sample (filled circle in Fig. 5c) is similar to values found in the youngest part of CF7-PC33. Both the MAR and ACL_{24-26} exhibit significant correlations with several other proxies (Table 2). The MAR of Fe (MAR_{Fe}) shows relatively low and high accumulations before 760 and after 730 cal yr BP (Fig. 5d; Rebolledo et al., 2008). For each interval, a rather constant decrease is observed towards the top of the record (Figs. 5d).

Alkenone-derived SST varies between 9.8 and 13.3°C over the entire time span and oscillates between 11.7 and 13.3°C before 1080 cal yr BP (Fig 5e). Thereafter, temperatures display a general cooling trend with two distinct intervals of lower temperatures (~10°C) between 800 and 500 cal yr BP and between 500 and 120 cal yr BP (Fig. 5e). Alkenone-derived SST from the sediment surface (11.8°C; Fig. 5e) resembles present-day SST of the area during spring time (Rojas et al., 2005).

DISCUSSION

Interpretation of proxies

The MS is directly related to the mineral content of the sediment and can therefore be used as a physical sedimentary proxy for the terrestrial supply of siliciclastic sediments. In our record, the higher MS values after 900 cal yr BP may be interpreted as a relatively

281 higher supply of siliciclastic sediments (Fig. 3a), in agreement with an increase in the bulk
282 sedimentation rate (Fig. 2).

283 Elemental and isotopic analyses in surface sediments of northern Patagonia fjords
284 exhibit a linear mix of allochthonous and autochthonous organic matter from open ocean
285 areas to the fjord heads (Sepúlveda, 2005). This interpretation is based on the characteristic
286 elemental and isotopic signatures found in marine and terrestrial organic matter, which
287 have been widely used as tracers of organic matter sources in marine and fresh water
288 systems (e.g., Thornton and McManus, 1994; Meyers, 1997). We interpret our proxy data
289 in terms of relative changes in the sources of organic matter into the system. Therefore,
290 higher C/N ratios resulting from a higher input of terrigenous material would be
291 accompanied by more depleted $\delta^{13}C$ and $\delta^{15}N$. This is reflected in the significant inverse
292 correlation observed between the C/N ratio and $\delta^{13}C$ and $\delta^{15}N$, most notably before 400 cal
293 yr BP (Table 2). We assume that changes in terrestrial input are mostly controlled by
294 continental precipitation and runoff, whereas changes in marine organic matter
295 contributions are controlled by marine productivity. The general trend of the three
296 parameters point to reduced terrestrial contributions before 900 cal yr BP (Figs. 3b,c,d),
297 interpreted as a consequence of less rainfall, while increased input of terrestrial organic
298 matter after 750 cal yr BP reflects increased runoff derived from more precipitation (Figs.
299 3b,c,d). The latter would explain the higher sedimentation rate observed during the last 730
300 years (Fig. 2). However, the relationship among these three proxies can be complex. For
301 instance, the increase in the C/N ratio between 1600 and 1400 cal yr BP has no parallel
302 with other proxies (Fig. 3), possibly due to preferential removal of nitrogen-rich material
303 during early diagenesis (Meyers, 1997 and references therein). Additionally, the trends

observed between 450 and 200 cal yr BP (Fig. 3) suggest that variations in organic matter sources alone can not explain such distributions. The long-term depletion observed in the $\delta^{13}C$ record between 420 and 135 cal yr BP may also be influenced by changes in marine primary productivity (Meyers, 1997) which, according to Rebolledo et al. (2008), has increased after 750 cal yr BP in response to higher continental runoff. On the other hand, the $\delta^{15}N$ excursion between 400 and 200 cal yr BP appears to run independently from the other proxies and cannot be explained by a change in terrestrial input (Fig. 3). Although water column denitrification and decreased fractionation during nutrient assimilation by phytoplankton could ultimately enrich sedimentary nitrogen (Gruber, 2004), no evidence of low oxygen or depletion of nutrients has been found to account for those possibilities. In order to minimize potential biases from a single analysis on the interpretation of these proxies we focus in the integrative multi-proxy signature of the terrestrial index (TI).

Integrated terrestrial signal

In order to further evaluate temporal changes in terrestrial sediment supply we compare the TI, obtained from proxies independent of changes in sedimentation rate, with the MAR_{waxes} and MAR_{Fe}. Additionally, we use the ACL of leaf waxes to evaluate changes in plant physiology due to variations in humidity. The TI defines two main different modes of precipitation for the entire record – relatively dry conditions before 950 cal yr BP and relatively humid conditions after 750 cal yr BP, separated by a two-step and rapid (~200 years) transition (Fig. 5a) coincident with the end of the MCA (e.g. Lamb, 1965). Higher terrestrial input and precipitation during the last 750 years can also be inferred from the MAR_{waxes} (Fig. 5b). Long-chain *n*-alkyl lipids are major components of epicuticular leaf

waxes from vascular plants (Eglinton and Hamilton, 1967) and have been widely used as indicators of the input of vascular land-plants in aquatic environments (e.g., Ohkouchi et al., 1997; Huang et al., 1999) due to their good preservation and slow remineralization rates (Haddad et al., 1992; Canuel and Martens, 1996). Thus, MAR_{waxes} represents a specific proxy for land-plant derived material that is directly related to on-land precipitation and continental runoff. The decrease in the ACL_{24-26} index from ~900 cal yr BP to the present-day is another indication of more humid/colder conditions less favorable for evaporation and water loss in plants (Fig. 5c). The ACL has been shown to increase latitudinally in response to decreased humidity and increased temperature, possibly as a protection against water loss (e.g., Sachse et al., 2006). The overall range of ACL variability was ~0.3 carbon units (Fig. 5c), which although low is remarkable for this area of high precipitation entirely dominated by C_3 plants. Abrupt vegetation changes observed during the last deglaciation in northern South America, where C_4 plants also occur, resulted in ACL_{24-28} differences of 0.4-0.5 (Hughen et al., 2004). Since the vegetation in northern Patagonia was dominated by an evergreen *Nothofagus* forest during the time scale covered by our study (Villagrán, 1988), we interpret our results as a physiological adaptation within the C_3 vegetation to control the water balance during periods of changing humidity and temperature. Higher ACL values would be indicative of relatively warm/dry conditions for the period before 950 cal yr BP, in good agreement with other proxies (Fig. 5).

Fe can be used as a proxy for terrigenous sediment supply since it occurs nearly exclusively in the inorganic fraction of the sediment, i.e., mainly in the soils covering the Andes. MAR_{Fe} illustrates two well-defined periods of relatively low and high terrestrial input before and after 720 cal yr BP, respectively (Fig. 5d; Rebolledo et al., 2008). The increase of MAR_{Fe} and MAR_{waxes} observed at 720 cal yr BP is primarily controlled by the

increase in the bulk sedimentation rate derived from the age model, which might be biased by the high uncertainty of the AMS-^{14}C dating at 9.5 cm (Table 1). However, we interpret this change as real since it parallels closely the main variation in the TI and ACL (Fig. 5).

Climatic variability in northern Patagonia and regional connections

The TI obtained from the PCA, together with the alkenone-derived SST allows us to obtain an integrated view of the climatic variability in northern Patagonia during the last 1,750 years. The two well-defined intervals – reduced precipitation and warmer temperatures before 950 cal yr BP, and markedly higher precipitation and lower (albeit highly variable) temperatures after 750 cal yr BP – are separated by a rapid transition of ~200 years (Figs. 5 a and e). The drop in SST is part of a smooth and long-term cooling trend starting at about 1075 cal yr BP (arguably at 1270 cal yr BP; Fig. 5e) and is consistent with a marine record obtained off the coast of northern Patagonia (Mohtadi et al., 2007), although exhibiting a higher amplitude. The sustained cooling of ~3°C between 1075 and 675 cal yr BP, which includes the transition from relatively drier to wetter conditions, represents about 50% of the difference observed between the Last Glacial Maximum and the Holocene at 41°S off the coast of Chile (~ 6°C; Lamy et al., 2004). Even though SST variability in semi-restricted coastal environments such as fjords can be amplified, such a difference on a time scale of centuries highlights the presence of abrupt and conspicuous climate variability during the last two millennia at this location. The transition from drier/warmer to wetter/colder conditions appears to coincide with the MCA, whereas cold (albeit variable) temperatures between 450 and 250 cal yr BP correspond to the interval defined for the LIA (Fig. 6). The reasonably good correspondence between precipitation and SST may be explained by changes in the intensity and/or core position of the SWW

belt (e.g., Lamy et al., 2002; Mohtadi et al., 2007), which is the main source of precipitation on the western side of southern South America (Strub et al., 1998). Therefore, wetter/colder conditions after 900 cal yr BP suggest an equatorward position of the SWW.

An important component of the global climate system is the ENSO, a coupled ocean-atmosphere phenomenon which originates in the tropical-subtropical eastern Pacific region and propagates to mid- to high latitudes via teleconnection patterns (e.g. Philander, 1990). Recent proxy records from both sides of the Andes have provided new insights into the connection between climate variability in northern Patagonia, tropical climate systems, and ENSO activity (Ariztegui et al., 2007; Mohtadi et al., 2007). A high-resolution record of El Niño-related flood events in Peru suggests extreme drought conditions between 1250 and 750 cal yr BP that has been interpreted as a period of persistently weak El Niño variability during the MCA (Fig. 6a; Rein et al., 2004). This period coincides with an observed long-term smooth decrease in SST in our record, as well as in another marine record offshore from the Patagonian fjord system at 44°S (Mohtadi et al., 2007; Figs. 6e,f). The Rein et al. (2004) record also suggests a transition from low to high El Niño activity around 800 cal yr BP that agrees with the final major shift in terrestrial input observed in our record (Fig. 6). A transition to high El Niño activity would imply the presence of a weaker southeast Pacific high-pressure (SPA) cell and, thus, an equatorward displacement of the SWW (e.g., Aceituno, 1988). The high variability observed in Peru before 1250 cal yr BP is not seen in our record (Fig. 6) and has been suggested to reflect different boundary conditions for ENSO before 1300 cal yr BP compared to the interval after 750 cal yr BP (Mohtadi et al., 2007).

High frequencies of flood events have been observed during the last 1000 years in Laguna Aculeo in central Chile (33°50'S; Fig. 6b; Jenny et al., 2002). These events have

399 been associated with increased winter precipitation and frontal system activity in central
400 Chile resulting from an intensification and/or equatorward displacement of the SWW and a
401 weakened SPA cell, likely in relation to ENSO variability (Jenny et al., 2002). Periods with
402 more intensive flooding were observed during the intervals 1750-1550, 1450-1250, 650-
403 250, and 100-20 cal yr BP (cross-hatched bars in Fig. 6b), with the highest number of
404 events occurring in the last 1000 years. The simultaneous changes in precipitation in central
405 and northern Patagonia evidence a close connection between both areas reflecting their
406 sensitivity to latitudinal shifts of the SWW. However, the intense flood events and high
407 ENSO variability observed in Laguna Aculeo (Jenny et al., 2002) and Peru (Rein et al.,
408 2004) before 1200 cal yr BP are not manifested at 44°S (Fig. 6). Although present-day
409 wind and precipitation anomalies in southern Chile are affected by ENSO variability (e.g.,
410 Montecinos and Aceituno, 2003; Schneider and Gies, 2004), contrasting responses can be
411 found north and south of 45°S (Schneider and Gies, 2004). This latitudinal boundary is
412 close to the coring location of this study and may have migrated latitudinally before 1200
413 cal yr BP, thus changing the present-day conditions and response to El Niño variability.
414 This latter issue raises awareness that ENSO-related climate variability in northern
415 Patagonia in the past can be difficult to assess.

416 Tree ring-derived summer temperature reconstructions of the last 1000 years from
417 northern Patagonia (41°S) have yielded evidence of cold intervals coincident with glacier
418 advances around 1050-880 and 680-280 cal yr BP (gray bars in Fig. 6c), in close
419 relationship to ENSO activity and a weaker SPA (Villalba, 1994). In Lake Puyehue at 40°S,
420 high precipitation and increased productivity between 450 and 250 cal yr BP has been
421 interpret as the local signature of the LIA (Bertrand et al., 2005). Our SST record exhibits
422 two distinct cold intervals around 670 and 450-250 cal yr BP; the latter includes the period

423 defined by the LIA (Fig. 6f) suggesting a regional expression of this event. On the other
424 hand, a warm interval inferred between 870 and 700 cal yr BP (Villalba, 1994), i.e. roughly
425 coincident with the end of the MCA (black bar in Fig. 6c), is concurrent with the major
426 transition in SST and terrestrial input in our record (Fig. 6).

427 Humid conditions during the LIA and less humid conditions during the MCA at
428 41°S off Chile have been associated with latitudinal shifts of the SWW primarily controlled
429 by changes within tropical climate (i.e. the Hadley cell intensity) and possibly including
430 ENSO effects (Lamy et al., 2001). However, multi-centennial variability in SST and sea
431 surface salinity (SSS) in this area is controlled by temperature changes in Antarctica
432 affecting the Antarctic Circumpolar Current (ACC; Lamy et al., 2002). Lamy et al. (2002)
433 described SSTs warmer than present-day values before 850 cal yr BP, after which a
434 constant decrease was observed until the present (Fig. 6d). The latter cooling was followed
435 by lower salinities between 850 and 750 cal yr BP as part of a long-term decrease (Fig. 6d).
436 Mohtadi et al. (2007) calculated a 2° northward shift in the position of the SWW between
437 1300 and 750 cal yr BP based on SST, SSS, and marine productivity records at 44°S off the
438 coast of Chile (Fig. 6e). These authors suggest an equatorward displacement of the SWW
439 resulting from ENSO variability between 1300 and 750 cal yr BP as seen in Peru (Rein et
440 al., 2004) and other locations, leaving the area under cold and humid conditions. Due to its
441 location in the inner fjord system, our core recorded continental changes in precipitation
442 and temperature mostly due to variability in the storm track of the SWW, in contrast to the
443 mixed influence of the SWW and the ACC reported at open ocean sites (Lamy et al., 2002;
444 Mohtadi et al., 2007). Salinity changes off northern Patagonia are influenced by the low-
445 salinity surface Chilean Fjord Water (CFW; e.g., Lamy et al., 2002). Although the CFW
446 can exit the northern Patagonia fjord area through several channels, the main output is

through the “Boca del Guafo” (Fig. 1b; Silva et al., 1995). This would explain why the transition to a wet period around 900 cal yr BP is observed as a salinity anomaly off 41°S (Lamy et al., 2002) but is absent off 44°S (Mohtadi et al., 2007; Fig. 6). Although differences in the timing of events exist (most likely due to dissimilar reservoir ages and materials used for ^{14}C dating), the integrated data from our record and adjacent areas indicate a consistent pattern of cold/humid conditions during the last millennia associated with an equatorward displacement of the SWW (Fig. 6).

Hydrographic changes on the shelf of the western Antarctic Peninsula (i.e., ODP Hole 1098B at Palmer Deep; Shevenell and Kennett, 2002) respond to variability in the strength and/or position of the SWW due to atmospheric perturbations in the low-latitude tropical Pacific. Evidence from Palmer Deep suggests a transition to cold conditions and an intensification of the SWW starting at about 1250 cal yr BP and reaching a maximum at 850 cal yr BP (Fig. 6h). This intensification predates the main changes in terrestrial input in our record but coincides with the smooth, long-term decrease in SST (Fig. 6). This decrease in SST has been also described offshore the fjord system at 44°S, where it is related to ENSO (Fig. 6e; Mohtadi et al., 2007), hence demonstrating the presence of teleconnections between northern Patagonia and high- and low-latitudes.

The reasonably good correlation between our results (particularly SST) and other continental and marine archives from central-south Chile, Peru, and Antarctica corroborates the sensitivity of northern Patagonia for tracking latitudinal shifts of the SWW. This correspondence also confirms the occurrence of globally important climatic anomalies such as the MCA and the LIA, as well as ENSO-related climatic variability, within the northern Patagonia region.

Acknowledgements

The preparation of this article was made possible by the support of the Comité Oceanográfico Nacional Chile through the Special Fund to Promote Interdisciplinary Publications of the CIMAR Program. Sampling was funded by the CIMAR FIORDO-7 Program (Grant CPF 01-10). We thank the Servicio Hidrográfico y Oceanográfico de la Armada de Chile and the captain and crew of the AGOR Vidal Gormaz for their professional help during the CIMAR FIORDO-7 expedition, the EULA Center at University of Concepción (UDEC) for logistic support, and the NOSAMS at Woods Hole Oceanographic Institution (WHOI) for ^{14}C dating. We also thank C. Bertrand, D. Montlucon, L. Nuñez, and L. Xu for laboratory assistance; P. Vera for logistic assistance; and M. Mohtadi for fruitful discussion. Drs. F. Lamy and J. Kaiser are acknowledged for constructive reviews. J. Sepúlveda was funded by a M.Sc. scholarship from the Graduate School of UDEC and by Fundación Andes through the WHOI/UDEC agreement during a research visit at WHOI. S. Bertrand acknowledges the Belgian American Educational Foundation and the Marie Curie actions of the European Union for funding his postdoctoral stay at WHOI. N.J. Drenzek acknowledges the ODP Schlanger and U.S. EPA STAR fellowships whilst at WHOI. This work was funded by the Center for Oceanographic Research in the eastern South Pacific (COPAS) and grant Semilla-Patagonia # 206.112.097-1sp of UDEC.

493 Table 1. Radiocarbon dates from core CF7-PC33

Laboratory code	Core depth (cm)	Material	^{14}C-AMS age (yr BP)	± Error (yr)	Calibrated age (cal yr BP)	± Error (1σ) (yr)
OS-38629	9.5	leaf fragment	125	212	142	200
OS-38308	81.75	wood fragment	850	100	730	102
OS-38361	133.8	wood fragment	1550	30	1375	44
OS-38362	167.7	leaf fragment	1890	35	1771	67

494

495

496

Table 2. Pearson correlation matrix for the entire record (above), and for the period before 450 cal yr BP (below). The latter was performed to discuss the effect of the positive $\delta^{15}N$ excursion observed between 200 and 400 cal yr BP (see text).

Variables	C/N	$\delta^{13}C$	$\delta^{15}N$	MAR_{waxes}	ACL_{24-26}
C/N	**1.00**				
$\delta^{13}C$	**-0.51**	**1.00**			
$\delta^{15}N$	**-0.30**	0.03	**1.00**		
MAR_{waxes}	**0.58**	**-0.56**	-0.08	**1.00**	
ACL_{24-26}	**-0.49**	**0.59**	0.08	**-0.64**	**1.00**

Variables	C/N	$\delta^{13}C$	$\delta^{15}N$	MAR_{waxes}	ACL_{24-26}
C/N	**1.00**				
$\delta^{13}C$	**-0.51**	**1.00**			
$\delta^{15}N$	**-0.60**	**0.58**	**1.00**		
MAR_{waxes}	**0.54**	**-0.49**	**-0.41**	**1.00**	
ACL_{24-26}	**-0.54**	**0.45**	**0.36**	**-0.66**	**1.00**

Values in bold are significantly different from 0 with a significance level alpha = 0.05

C/N = Molar C/N ratio

$\delta^{13}C$ = Carbon isotopic composition of organic matter

$\delta^{15}N$ = Nitrogen isotopic composition of decalcified sediments

MAR_{waxes} = Mass accumulation rate of leaf waxes (mg m^{-2} y^{-1})

ACL_{24-26} = Average chain length between *n*-C_{24} and *n*-C_{26} fatty acids

509 References

510 Abarzúa, A.M., Villagrán, C., Moreno, P.I., 2004. Deglacial and postglacial climate history
511 in east-central Isla Grande de Chiloé, southern Chile (43°S). Quaternary Research
512 62**,** 49-59.
513 Aceituno, P., 1988. On the Functioning of the Southern Oscillation in the South American
514 Sector. Part I: Surface Climate. Monthly Weather Review 116**,** 505-524.
515 Ariztegui, D., Bösch, P., Davaud, E., 2007. Dominant ENSO frequencies during the Little
516 Ice Age in Northern Patagonia: The varved record of proglacial Lago Frías,
517 Argentina. Quaternary International 161**,** 46-55.
518 Barker, P.F., Camerlenghi, A., Acton, G.D., 1999. "Proceedings of the Ocean Drilling
519 Program, Initial Reports, vol. 178." Ocean Drilling Program, College Station,
520 Texas.
521 Benn, D.I., Clapperton, C.M., 2000. Glacial sediment-landform associations and
522 paleoclimate during the Last Glaciation, Strait of Magellan, Chile. Quaternary
523 Research 54**,** 13-23.
524 Bertrand, S., Boës, X., Castiaux, J., Charlet, F., Urrutia, R., Espinoza, C., Lepoint, G.,
525 Charlier, B., Fagel, N., 2005. Temporal evolution of sediment supply in Lago
526 Puyehue (Southern Chile) during the last 600 yr and its climatic significance.
527 Quaternary Research 64**,** 163-175.
528 Brassell, S.C., Eglinton, G., Marlowe, I.T., Pflaumann, U., Sarnthein, M., 1986. Molecular
529 stratigraphy: a new tool for climatic assessment. Nature 320**,** 129-133.
530 Canuel, E.A., Martens, C.S., 1996. Reactivity of recently deposited organic matter:
531 Degradation of lipid compounds near the sediment-water interface. Geochimica et
532 Cosmochimica Acta 60**,** 1793-1806.
533 Dávila, P.M., Figueroa, D., Müller, E., 2002. Freshwater input into the coastal ocean and its
534 relation with the salinity distribution off austral Chile (35-55°S). Continental Shelf
535 Research 22**,** 521-534.
536 Delgado, S., 2004. Relación entre el perfil del basamiento de fiordos y canales y la
537 morfoestructura regional en Norpatagonia. Unpublished MSc. thesis, Universidad
538 de Chile, Chile.
539 deMenocal, P.B., Bond, G.C., 1997. Holocene climate less stable than previously thought.
540 EOS 78, 447-450.
541 DGA, 2003. Dirección General de Aguas, Chile (http://www.dga.cl).
542 Domack, E.W., Mayewski, P.A., 1999. Bi-polar ocean linkages: evidence from late-
543 Holocene Antarctic marine and Greenland ice-core records. The Holocene 9**,** 247-
544 251.
545 Eglinton, G., Hamilton, R.J., 1967. Leaf epicuticular waxes. Science 156**,** 1322-1335.
546 Gruber, N., 2004. The dinamics of the marine nitrogen cycle and its influence on
547 atmospheric CO_2 variations. *In:* Follows, M., Oguz, T. (Eds.), The Ocean Carbon
548 Cycle and Climate. Kluwer Academis Publishers, London, pp. 97–148.
549 Haddad, R.I., Martens, C.S., Farrington, J.W., 1992. Quantifying early diagenesis of fatty
550 acids in a rapidly accumulating coastal marine sediment. Organic Geochemistry 19**,**
551 205-216.
552 Haug, G.H., Hughen, K.A., Sigman, D.M., Peterson, L.C., Rohl, U., 2001. Southward
553 migration of the Intertropical Convergence Zone through the Holocene. Science
554 293**,** 1304-1308.

555 Huang, Y., Street-Perrott, F.A., Perrott, R.A., Metzger, P., Eglinton, G., 1999. Glacial-
556 interglacial environmental changes inferred from molecular and compound-specific
557 $\delta^{13}C$ analyses of sediments from Sacred Lake, Mt. Kenya. Geochimica et
558 Cosmochimica Acta 63**,** 1383-1404.
559 Hughen, K.A., Eglinton, T.I., Xu, L., Makou, M., 2004. Abrupt tropical vegetation
560 response to rapid climate changes. Science 304**,** 1955-1959.
561 Jenny, B., Valero-Garcés, B.L., Urrutia, R., Kelts, K., Veit, H., Appleby, P.G., Geyh, M.,
562 2002. Moisture changes and fluctuations of the Westerlies in mediterranean central
563 Chile during the last 2000 years: The Laguna Aculeo record (33°50'S). Quaternary
564 International 87**,** 3-18.
565 Kreutz, K.J., Mayewski, P.A., Meeker, L.D., Twickler, M.S., Whitlow, S.I., Pittalwala, I.I.,
566 1997. Bipolar changes in atmospheric circulation during the Little Ice Age. Science
567 277**,** 1294-1296.
568 Lamb, H.H., 1965. The early medieval warm epoch and its sequel. Palaeogeography,
569 Palaeoclimatology, Palaeoecology 1**,** 13-37.
570 Lamy, F., Hebbeln, D., Röhl, U., Wefer, G., 2001. Holocene rainfall variability in southern
571 Chile: a marine record of latitudinal shifts of the Southern Westerlies. Earth and
572 Planetary Science Letters 185**,** 369-382.
573 Lamy, F., Kaiser, J., Ninnemann, U., Hebbeln, D., Arz, H.W., Stoner, J., 2004. Antarctic
574 timing of surface water changes off Chile and Patagonian ice sheet response.
575 Science 304**,** 1959-1962.
576 Lamy, F., Rühlemann, C., Hebbeln, D., Wefer, G., 2002. High- and low-latitude climate
577 control on the position of the southern Peru-Chile Current during the Holocene.
578 Paleoceanography 17, doi:10.1029/2001PA000727.
579 Lara, A., Villalba, R., 1993. A 3620-year temperature record from Fitzroya cupressoides
580 tree rings in southern South America. Science 260**,** 1104-1106.
581 Luckman, B.H., Villalba, R., 2001. Assessing the synchroneity of glacier fluctuations in the
582 Western Cordillera of the Americas during the last millenium. *In:* Markgraf, V.
583 (Ed), Interhemispheric Climate Linkages. Academic Press, San Diego, pp. 119-137.
584 Mayewski, P.A., Rohling, E.E., Curt Stager, J., Karlén, W., Maasch, K.A., David Meeker,
585 L., Meyerson, E.A., Gasse, F., van Kreveld, S., Holmgren, K., Lee-Thorp, J.,
586 Rosqvist, G., Rack, F., Staubwasser, M., Schneider, R.R., Steig, E.J., 2004.
587 Holocene climate variability. Quaternary Research 62**,** 243-255.
588 Meyers, P.A., 1997. Organic geochemical proxies of paleoceanographic, paleolimnologic,
589 and paleoclimatic processes. Organic Geochemistry 27**,** 213-250.
590 Moberg, A., Sonechkin, D.M., Holmgren, K., Datsenko, N.M., Karlen, W., 2005. Highly
591 variable Northern Hemisphere temperatures reconstructed from low- and high-
592 resolution proxy data. Nature 433**,** 613-617.
593 Mohtadi, M., Romero, O.E., Kaiser, J., Hebbeln, D., 2007. Cooling of the southern high
594 latitudes during the Medieval Period and its effect on ENSO. Quaternary Science
595 Reviews 26**,** 1055-1066.
596 Montecinos, A., Aceituno, P., 2003. Seasonality of the ENSO-Related Rainfall Variability
597 in Central Chile and Associated Circulation Anomalies. Journal of Climate 16**,** 281-
598 296.
599 Ohkouchi, N., Kawamura, K., Kawahata, H., Taira, A., 1997. Latitudinal distributions of
600 terrestrial biomarkers in the sediments from the Central Pacific. Geochimica et
601 Cosmochimica Acta 61**,** 1911-1918.

Philander, S.G.H., 1990. "El Niño, La Niña and the Southern Oscillation." Elsevier, New York.

Pizarro, G., Astoreca, R., Montecinos, V., Paredes, M.A., Alarcón, G., Uribe, P., Guzmán, L., 2005. Patrones espaciales de la abundancia de la clorofila, su relación con la productividad primaria y la estructura de tamaños del fitoplancton en Julio y Noviembre de 2001 en la región de Aysén (43°- 46° S). Ciencia y Tecnología Marina 28**,** 27-42.

Prahl, F.G., Muehlhausen, L.A., Zahnle, D.L., 1988. Further evaluation of long-chain alkenones as indicators of paleoceanographic conditions. Geochimica et Cosmochimica Acta 52**,** 2303-2310.

Rebolledo, L., Sepúlveda, J., Lange, C.B., Pantoja, S., Bertrand, S., Hughen, K., Figueroa, D., 2008. Late Holocene marine productivity changes in Northern Patagonia-Chile inferred from a multi-proxy analysis of Jacaf channel sediments. Estuarine, Coastal and Shelf Science 80**,** 314-322.

Rein, B., Lückge, A., Sirocko, F., 2004. A major Holocene ENSO anomaly during the Medieval period. Geophysical Research Letters 31, doi:10.1029/2004GL020161.

Sachse, D., Radke, J., Gleixner, G., 2006. δD values of individual n-alkanes from terrestrial plants along a climatic gradient - Implications for the sedimentary biomarker record. Organic Geochemistry 37**,** 469-483.

Salamanca, M.A., Jara, B., 2003. Distribución y acumulación de plomo (Pb y ^{210}Pb) en sedimentos de los fiordos de la XI región de Chile. Ciencia y Tecnología del Mar 26**,** 61-71.

Schneider, C., Gies, D., 2004. Effects of El Nino-southern oscillation on southernmost South America precipitation at 53° S revealed from NCEP-NCAR reanalyses and weather station data. International Journal of Climatology 24**,** 1057-1076.

Sepúlveda, J., Pantoja, S., Hughen, K., Lange, C., Gonzalez, F., Muñoz, P., Rebolledo, L., Castro, R., Contreras, S., Ávila, A., Rossel, P., Lorca, G., Salamanca, M., Silva, N., 2005. Fluctuations in export productivity over the last century from sediments of a southern Chilean fjord (44°S). Estuarine, Coastal and Shelf Science 65**,** 587-600.

Sepúlveda., J., 2005. Terrigenous input in Northern Patagonia fjords: Geochemical evidence from recent and late Holocene sediments. Unpublished MSc. thesis, Universidad de Concepción, Chile.

Shevenell, A.E., Kennett, J.P., 2002. Antarctic Holocene climate change: A benthic foraminiferal stable isotope record from Palmer Deep. Paleoceanography 17, doi:10.1029/2000PA000596.

Silva, N., Maturana, J., Sepúlveda, J.I., Ahumada, R., 1998. Materia orgánica, C y N, su distribución y estequiometría, en sedimentos superficiales de la región norte de los fiordos y canales australes de Chile (crucero CIMAR-FIORDO 1). Ciencia y Tecnología del Mar 21**,** 49-74.

Silva, N., Prego, R., 2002. Carbon and Nitrogen Spatial Segregation and Stoichiometry in the Surface Sediments of Southern Chilean Inlets (41°-56°S). Estuarine, Coastal and Shelf Science 55**,** 763-775.

Silva, N., Sievers, H., Prado, R., 1995. Caracteristicas oceanográficas y una proposición de circulación para algunos canales australes de Chile entre 41°20’S y 46°40’S. Revista de Biología Marina 30**,** 207-254.

Stine, S., 1994. Extreme and persistent drought in California and Patagonia during mediaeval time. Nature 369**,** 546-549.

Stine, S., 2000. On the Medieval Climatic Anomaly. Current Anthropology 41**,** 627-628.
Strub, P.T., Mesías, J., Montecino, V., Rutllant, J., Salinas, S., 1998. Coastal ocean circulation off Western South America. Coastal segment (6, E). *In:* Robinson, R.A., Brink, K.H. (Eds.), The Sea. J. Wiley & Sons, New York, pp. 273-313.
Thompson, L.G., Mosley-Thompson, E., Dansgaard, W., Grootes, P.M., 1986. The Little Ice Age as recorded in the stratigraphy of the tropical Quelccaya Ice Cap. Science 234**,** 361-364.
Thornton, S.F., McManus, J., 1994. Application of organic carbon and nitrogen stable isotope and C/N ratios as source indicators of organic matter provenance in estuarine systems: Evidence from the Tay Estuary, Scotland. Estuarine, Coastal and Shelf Science 38**,** 219-233.
Villagrán, C., 1988. Late Quaternary vegetation of southern Isla Grande de Chiloé, Chile. Quaternary Research 29**,** 294-306.
Villalba, R., 1994. Tree-ring and glacial evidence for the medieval warm epoch and the little ice age in southern South America. Climatic Change 26**,** 183-197.

FIGURE CAPTIONS

Figure 1. (a) Map of southern Chile (30-60°S) showing the location of the sampling area in the Chilean fjords and other records mentioned in the text; a lacustrine record from Laguna Aculeo (black square; Jenny et al., 2002), marine records (black circles) GeoB7186-3 (Mohtadi et al., 2007) and GeoB3313-1 (Lamy et al., 2002), and a tree-ring derived temperature record from northern Patagonia (white triangle; Villalba, 1994). Black arrows are a schematic representation of the Southern Westerly Winds (SWW), Antarctic Circumpolar Current (ACC), Cape Horn Current (CHC), and Peru-Chile Current (PCC) based on Strub et al. (1998). Isolines indicate annual mean SST (°C) distribution (http://www.cdc.noaa.gov/index.html). The rectangle identifies the area displayed in Figure b. (b) Map of northern Patagonia showing the position of core CF7-PC33 in the Jacaf Fjord.

Figure 2. Age/depth relationship for core CF7-PC33. Ages are expressed in calibrated years before present (cal yr BP) and vertical bars represent the standard deviation. The large error of the youngest measurement was probably due to the small size of the fragments, close to the limit for AMS analysis. See Table 1 for details.

Figure 3. Physical and geochemical properties of core CF7-PC33; (a) Magnetic susceptibility; (b) Molar C/N ratio; (c) $\delta^{13}C$ of organic carbon; (d) $\delta^{15}N$ of decalcified sediments. Y-axis in figures (c) and (d) is inverted to facilitate comparison with (b). Solid triangles on the lower X-axis represent the age control.

Figure 4. Principal component analysis of the C/N ratio, $\delta^{13}C$, and $\delta^{15}N$, used to study and visualize the correlation between variables indicating changes in the input of terrestrial

726 organic matter. X and Y axes represent loadings of factors 1 and 2, respectively. The
727 variance and accumulative variability for each factor are given in parentheses.
728
729 Figure 5. Proxies indicative of terrestrial input, and sea surface temperature. (a) Factor 1 of
730 the principal component analysis for the C/N ratio, $\delta^{13}C$, and $\delta^{15}N$, used as a terrestrial
731 index; (b) Mass accumulation rate of plant waxes; (c) *n*-$C_{24\text{-}26}$ Average Chain Length of
732 plant waxes (inverted scale); (d) Mass accumulation rate of Fe; (e) Alkenone-derived sea
733 surface temperature, where the filled square represents the temperature obtained from
734 surface sediments. The black, thick line corresponds to a 3-point running average. Solid
735 triangles on the lower X-axis represent the age control. The black arrow indicates the
736 interpretation of proxies. The vertical gray bar corresponds to the main transition period
737 described in the text.
738
739 Figure 6. Relevant paleoclimatic reconstructions along Peru, Chile, and Antarctica. (a)
740 Lithic concentration at site 106 KL off Peru (see Rein et al., 2004 for details), used to
741 reconstruct the continental input during El Niño events; (b) occurrence of flood events in
742 Laguna Aculeo (33º50'S) as an indicator of periods of increased precipitation and erosion
743 rates (Jenny et al., 2002); the horizontal white and hatched bars correspond to periods of
744 flood events and periods of increased frequency and intensity of flood events, respectively;
745 (c) schematic representation of summer tree-ring derived temperature for northern
746 Patagonia around 41°S (Villalba, 1994); (d) alkenone-derived sea surface temperature
747 (black line), and $\delta^{18}O$-derived sea surface salinity (gray line) obtained from core GeoB
748 3313-1 off 41°S (Lamy et al., 2002); (e) alkenone-derived sea surface temperature (black

749 line) and $\delta^{18}O$-derived sea surface salinity (gray line; scale without units, see reference
750 below) obtained from core GeoB 7186-3 off Chile at 44°S (Mohtadi et al., 2007); (f)
751 alkenone-derived sea surface temperature from this study, where the black line represents a
752 3-point running average. The solid square and the horizontal dashed line represents the
753 modern alkenone-derived sea surface temperature for spring obtained from surface
754 sediments; (g) Terrestrial index obtained as the factor 1 of the principal component analysis
755 for the C/N ratio, $\delta^{13}C$, and $\delta^{15}N$ (inverted scale to facilitate comparison with other
756 records). The thick black line represents a 3-point running average in which positive and
757 negative values denote wet and dry conditions, respectively; (h) magnetic susceptibility
758 from ODP Hole 1098B obtained from the Palmer Deep, Antarctic Peninsula (Barker et al.,
759 1999; Shevenell and Kennett, 2002), where the black thick curve correspond to a 9-point
760 running average. The vertical gray bar symbolizes the main transition period described in
761 the text. Black and grey horizontal bars in the upper panel depict the “Little ice age” and
762 the “Medieval climate anomaly”.

Figure 1

Click here to download Figure: Fig 1.pdf

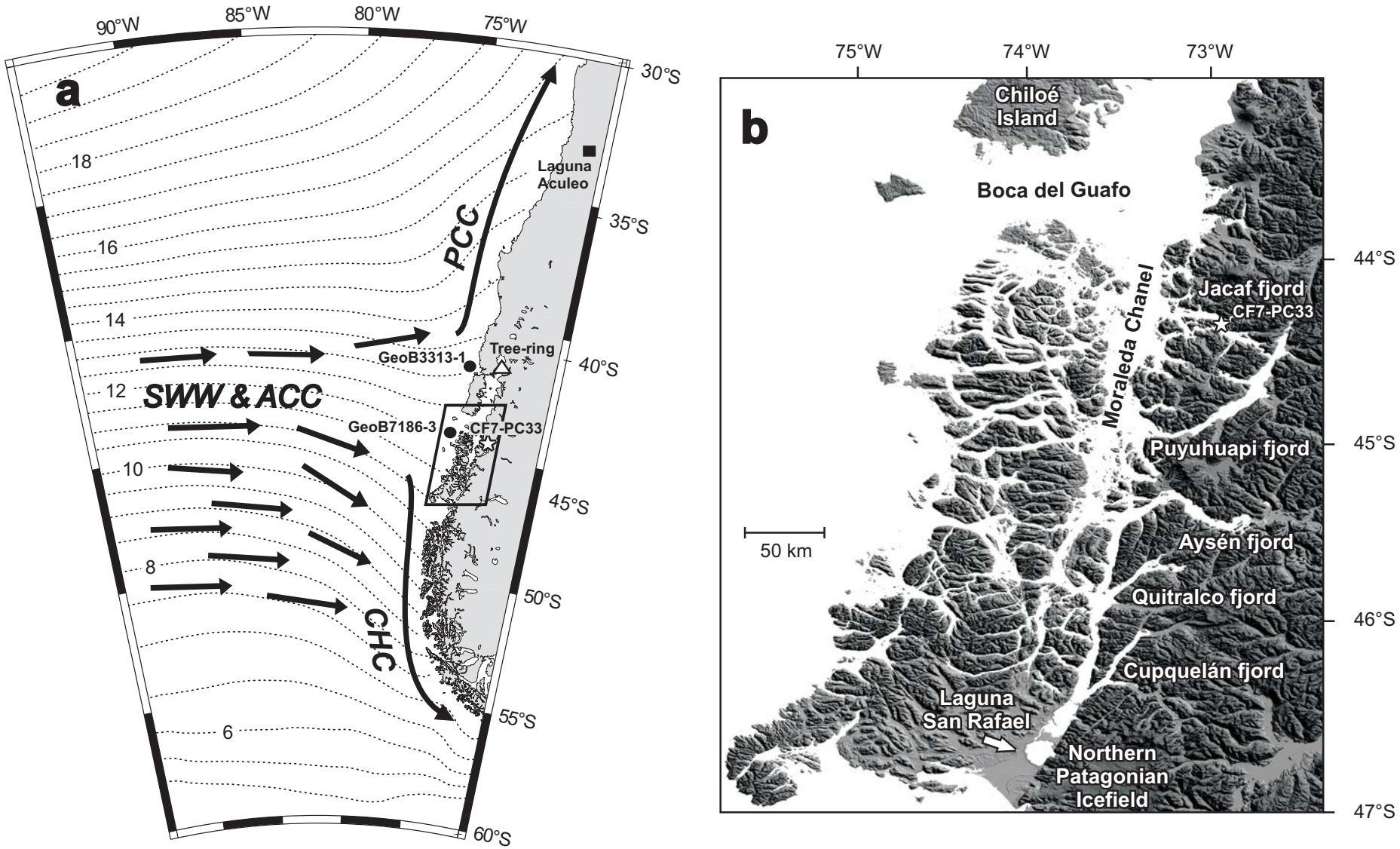

Figure 2

Click here to download Figure: Fig 2.pdf

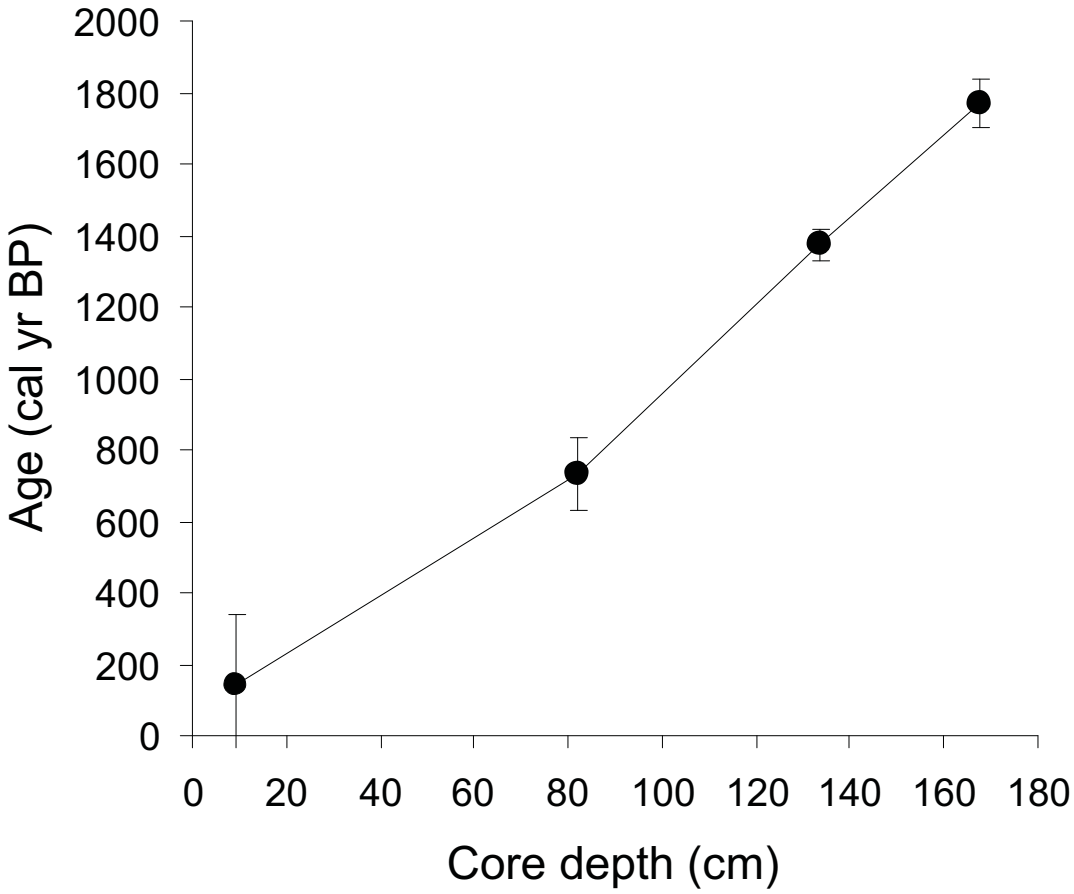

Figure 3

Click here to download Figure: Fig 3.pdf

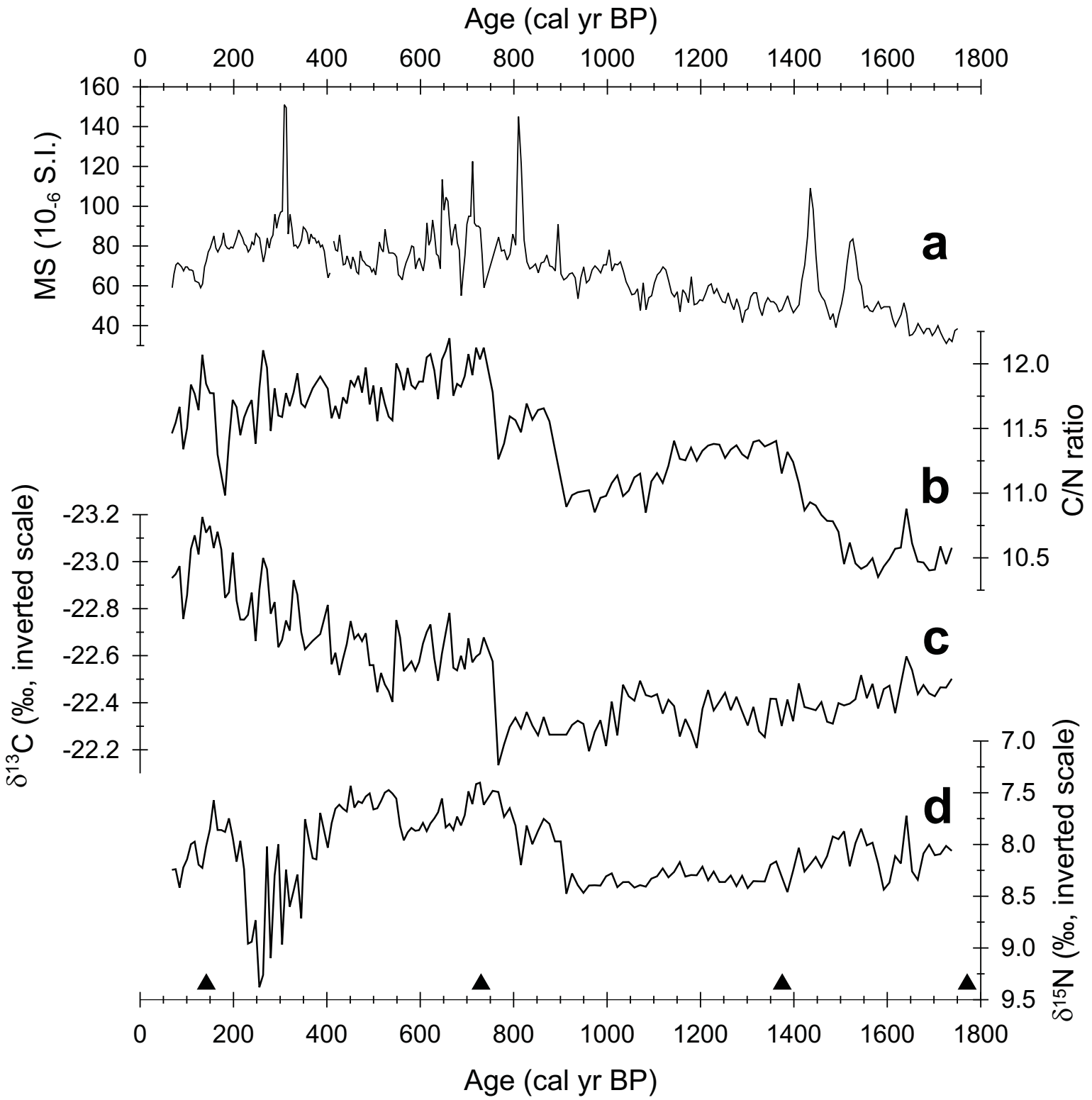

Figure 4

Click here to download Figure: Fig 4.pdf

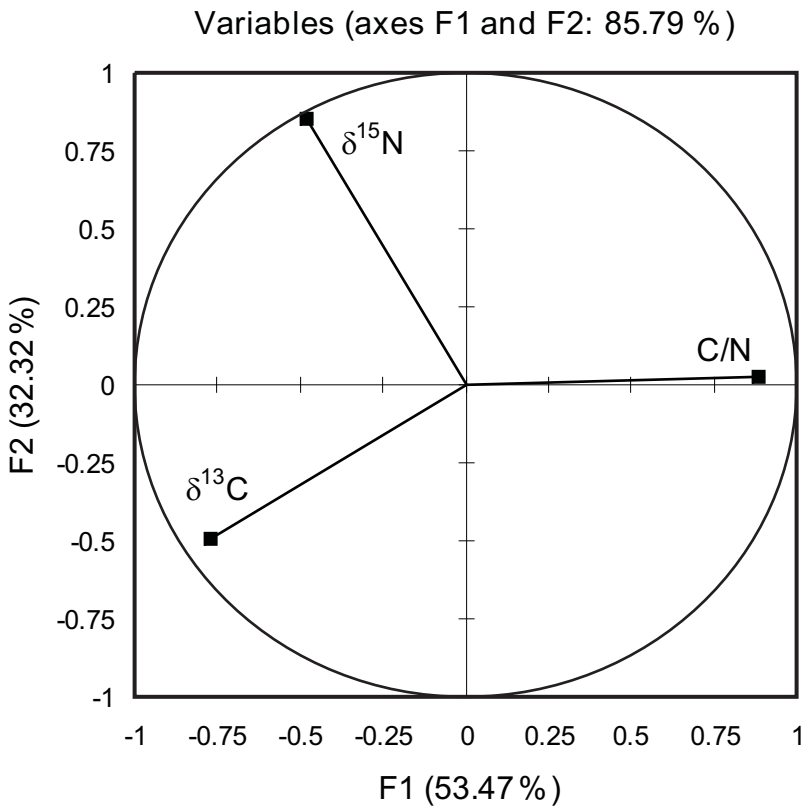

Figure 5

Click here to download Figure: Fig 5.pdf

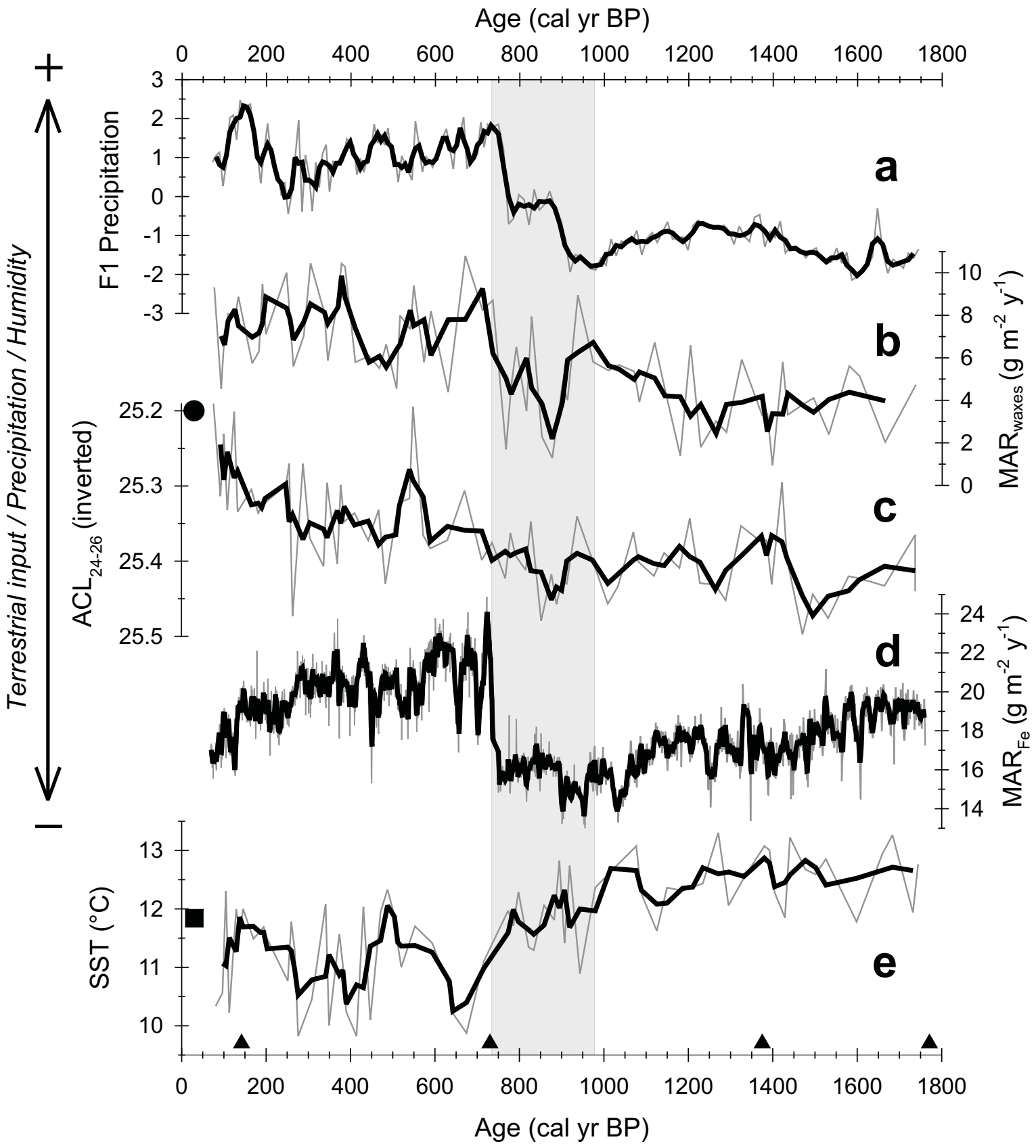

Figure 6

Click here to download Figure: Fig 6.pdf